Plasmonics (2022) 17:1921–1927
https://doi.org/10.1007/s11468-022-01675-y

Switchable Fano Resonance Filter with Graphen e-based Double Freestanding Dielectric Gratings

Zexiang Wang[1] · Wenjie Shi[1] · Zhengda Hu[1] · Jicheng Wang[1,2] · Sergei Khakhomov[3] · Igor Semchenko[3]

Received: 5 April 2022 / Accepted: 5 June 2022 / Published online: 20 June 2022

Abstract
Fano resonance is based on plasmonic metasurfaces and has many applications in all kinds of fields. In this paper, we propose an independently switchable double-layer raster structure based on graphene. Depending on the highly adjustable nature of graphene, the Fermi energy level can be adjusted to control the Fano resonance at different wavelengths. The equivalent resonator coupling mode method is used to simulate the Fano resonance, and the transmission spectrum fits well. Functional switch at different wavelengths can be achieved using Fano resonance technology. The simulation obtained a fantastic group refractive index of the designed structure, indicating that there is a possibility to apply it in slow light. The effect of the environmental refractive index on sensing performance was studied and we found the structure has great potential in making high-sensitivity sensors. To sum up, it is hoped that this structure can make a great contribution to the manufacture of integrated optics.

Keywords Fano resonance · Switchable · Graphene · Slow light · Sensor

Introduction

Fano resonance was originally quantum interference phenomena produced by discrete and continuous states in atomic physics [1, 2]. Researchers found that Fano resonance, formed by interferences in both discrete and continuous states, is also widespread in optical systems. This common optical phenomenon has quite a few applications in metal systems, such as optical switches [3, 4], light absorbers [5] and plasma-induced transparency (PIT) [6, 7]. PIT is a special type of Fano resonance, whose formation is led by the coherent interference of light wave patterns of different optical paths. Fano resonance has been widely used in various types of systems, including light filtering [8], slow light propagation [9], sensors [10], etc. Additionally, with the unique ability to concentrate electromagnetic energy on deep sub-wavelength scales, surface plasmons are the collective oscillations of electrons in metals which have a strong enhancement to local electric fields and better adaptability to nanostructure [11–13].

The Fano resonance can be achieved in metal or dielectric metamaterial structures. Since metal or dielectric metamaterial structures are difficult to modify after manufacturing, Fano resonance can only work within a preset frequency band or resonance frequency. One key advantage of graphene surface plasmons is that they can control optical responses by adjusting gating techniques, an external magnetostatic field or chemical potential [14]. The grating can be regarded as one of the simplest metamaterials in the grating coupling device, metal or semiconductor. When an electromagnetic wave is incident onto a grating, electromagnetic waves that match the wave vector conditions will have a strong effect on the grating, causing resonance. Regarding the application of Fano resonance, many teams have studied it. Zhou et al. studied two-dimensional photonic crystal plates that can be integrated into a variety of optics [15]. In 2014, Alonso-Gonzalez et al. controlled graphene plasma with resonant metal antennas and spatial conductivity modes [16]. 2019 witnesses that Wang et al. used coupled resonant model to analyze the absorption of silicon carbide gratings and plasma excitons on graphene surfaces [17].

✉ Jicheng Wang
jcwang@jiangnan.edu.cn

[1] School of Science, Jiangsu Provincial Research Center of Light Industrial Optoelectronic Engineering and Technology, Jiangnan University, Wuxi 214122, China

[2] State Key Laboratory of Applied Optics, Fine Mechanics and Physics, Changchun Institute of Optics, Chinese Academy of Sciences, Changchun 130033, China

[3] Departments of Optics, Francisk Skorina Gomel State University, 246019 Gomel, Belarus

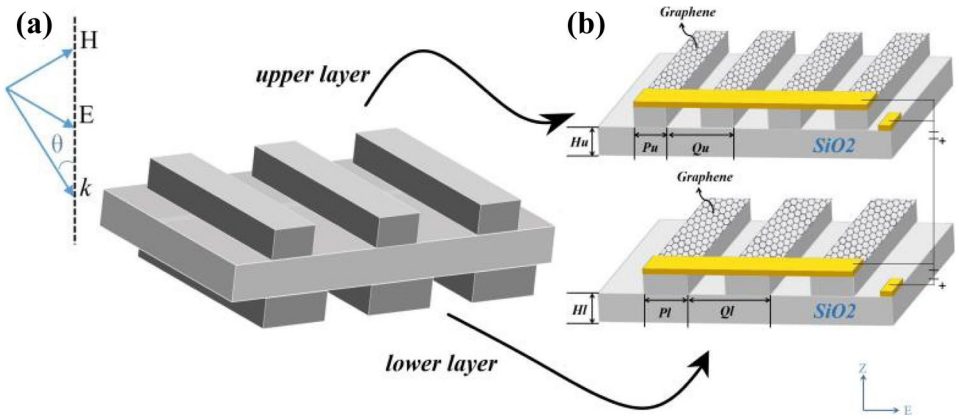

Fig. 1 **a** 3D schematic of the GDFDG structure and **b** schematic diagram of the grating period with geometric parameters, $P_u = 49.5$ nm, $Q_u = 90$ nm, $H_u = 50$ nm, $P_l = 70$ nm, $Q_l = 90$ nm and $H_l = 50$ nm, respectively. The Fermi energy levels of UGG and LGG are regulated by applying two independent bias voltages

In this paper, a switchable Fano resonance filter with graphene-based double freestanding dielectric gratings(GDFDG) was designed. With the geometric parameters of the structure changing, we achieved the target effect. Through the theoretical analysis of coupled-mode theory (CMT) [18–20], the result of the theoretical fit is basically consistent with the simulated numerical data. Based on the characteristics of Fano resonance, this structure can also be made into a near-field optical switch. Moreover, the refractive index data of the group obtained by numerical simulation indicate that GDFDG has good slow light capability and owing to the high sensitivity of GDFDG, high-quality sensors can also be realized.

Structure and Theory

Figure 1 shows a GDFDG hybrid system which is designed to investigate the Fano resonance. The periodic structure is divided into two parts, one part is an upper graphene grating with a Fermi energy level, and the other part is a lower graphene grating separated by a dielectric spacer of the Fermi energy level. In this paper, COMSOL software is in use to perform numerical simulation using the finite element method. During the simulation, silica with a dielectric constant of 3.9 [21] is employed as a substrate for the upper graphene grating(UGG) and the lower graphene grating(LGG). For the grating material is the same, the two grating substrates are combined and spliced together, as Fig. 1a shows. Meanwhile, period boundary conditions are used in both the x and y directions in our simulations. When a broadband plane wave is incident from the z direction, there is a perfectly matched layer along the z direction to absorb all the light that reaches the boundary. The graphene layer is constructed in the simulation as a boundary condition for surface currents and TM polarization waves are incident in the positive direction of the z-axis. On the basis of theoretical and experimental researches, the conductivity of graphene can be expressed by the Drude model [22]:

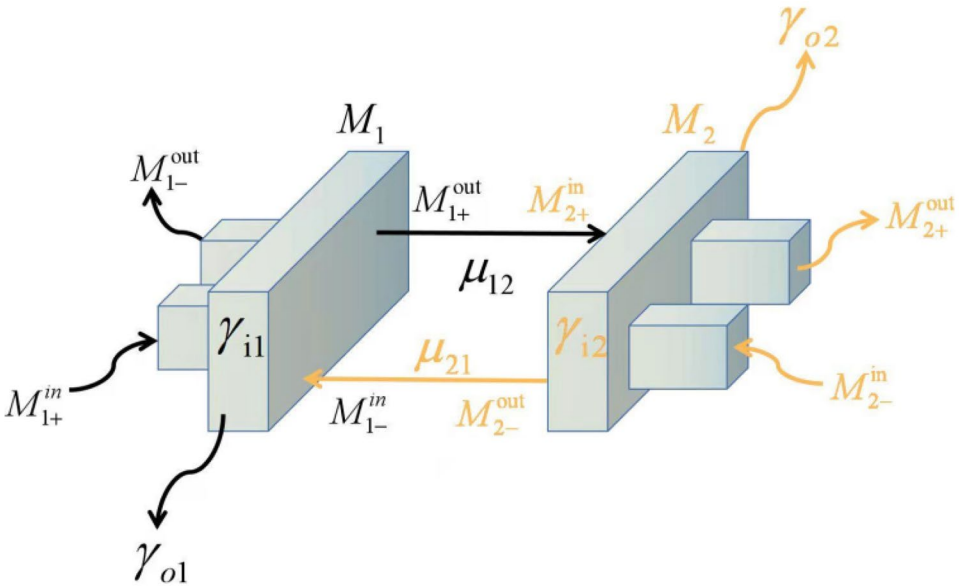

Fig. 2 Equivalent theoretically coupled model of graphene-based plasma resonators

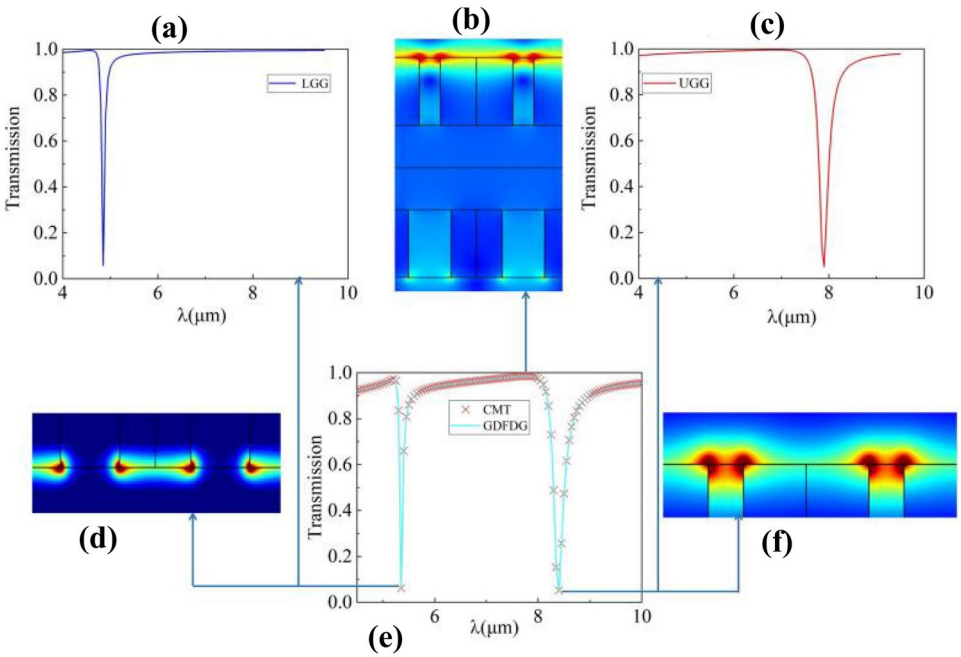

Fig. 3 **a**-**e** Transmission spectra of the LGG, the UGG and the GDFDG, respectively; **b** the electric field distribution of GDFDG at a wavelength of 7.55 μm; and **d**-**f** the electric field distribution of UGG and LGG at the Fano formant, when the Fermi energy levels of UGG and LGG are 0.6 eV and 0.9 eV, respectively

$$\sigma_g = \frac{ie^2 E_f}{\pi\hbar^2(\omega + i\tau^{-1})} \tag{1}$$

Here, ω, E_F and ħ are the angular frequency, the Fermi energy and the reduced Plank constant, respectively. The intrinsic relaxation time is expressed by $\tau = E_F\mu / ev_F^2$, where μ is the carrier mobility while Fermi velocity is $v_F \approx 10^6$ m/s. Recording to previous researches, at room temperature, the mobility of graphene films can reach 40,000 cm^2V^{-1} s^{-1} [23]. Therefore, considering the feasibility of the actual situation, μ is used as 15,000 cm^2V^{-1} s^{-1} in this paper, which is regarded as a right choice.

The energy can be coupled to the incidence of TM polarization waves into the GDFDG while the dynamic transmittance characteristics of the GDFDG can be solved by using the CMT. As Fig. 2 shows, there are two equivalent resonators named M_1, M_2 to serve as excitation state modes. Meanwhile, Min 1 ±, Min 2 ± represent the input amplitude of the incident wave and M out 1 ±, M out 2 ± are the output amplitude of the coupler reflected wave, respectively. The direction of propagation at the waveguide is expressed by M_+ and

$$M - \begin{pmatrix} \gamma_1 & -i\mu_{12} \\ -i\mu_{21} & \gamma_2 \end{pmatrix} \begin{pmatrix} M_1 \\ M_2 \end{pmatrix} = \begin{pmatrix} \sqrt{\frac{1}{\gamma_{o2}}} & 0 \\ 0 & \sqrt{\frac{1}{\gamma_{o2}}} \end{pmatrix} \begin{pmatrix} M_{1+}^{in} & M_{1-}^{in} \\ M_{2+}^{in} & M_2^{in} \end{pmatrix} \tag{2}$$

The above formula is used to represent the complex amplitude of these two resonators with $\gamma_I = (\ i\omega — i\omega_1 — 1/\gamma_{i1} — \gamma_{o1})$, $\gamma_2 = (\ i\omega — i\omega_2 — 1/\gamma_{i2} — \gamma_{o2})$. ω is the angular frequency and $\omega_{1/2}$ is resonant angular frequency. γ_{i1} and γ_{i2} are the inherent loss of UGG and LGG while μ_{12} and μ_{21} are the coupling coefficient between two modes. Hence, the

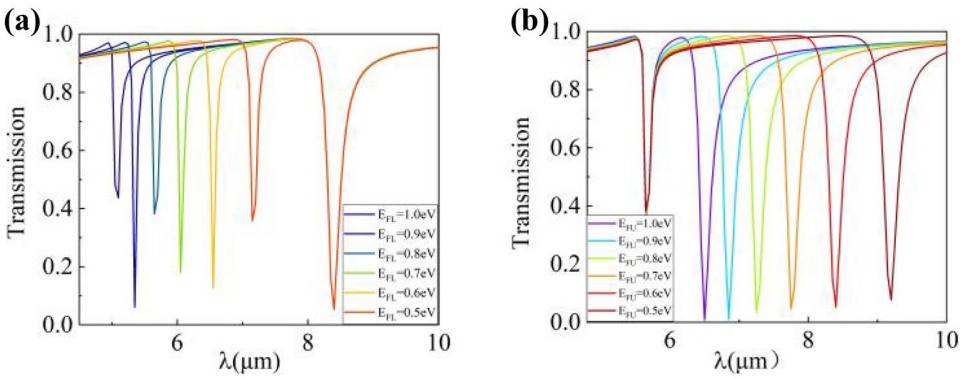

Fig. 4 **a** The transmission spectrum of GDFDG when changing the Fermi level of the LGG when $E_{FU} = 0.6$ eV and **b** the transmission spectrum of GDFDG when changing the Fermi level of the UGG when $E_{FL} = 0.8$ eV

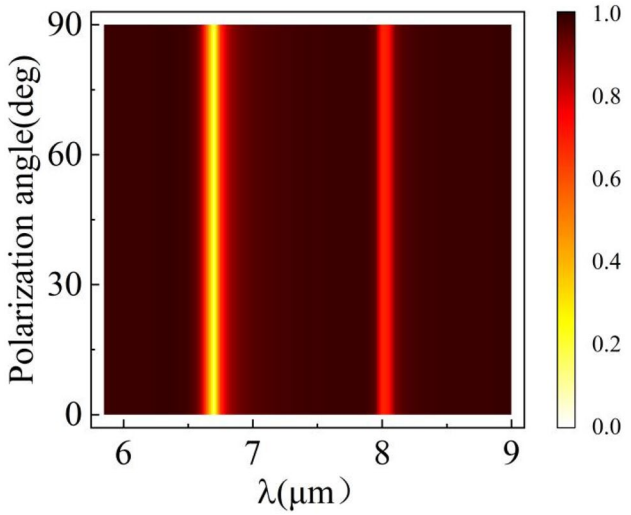

Fig. 5 Schematic diagram of the relationship between the polarization angle and light transmittance

coupling relationship between the two systems by the conservation of energy can be derived as below,

$$M_2^{in} = M_{1+}^{out} e^{i\phi}, M_1^{in} = M_{1-}^{out} e^{i\phi}, \tag{3}$$

$$\begin{aligned} M_{1+}^{out} &= M_{1+}^{in} - \sqrt{\frac{1}{\gamma_{o1}}} M_1, \\ M_{1-}^{out} &= M_{1-}^{in} - \sqrt{\frac{1}{\gamma_{o1}}} M_1, \end{aligned} \tag{4}$$

$$\begin{aligned} M_{2+}^{out} &= M_{2+}^{in} - \sqrt{\frac{1}{\gamma_{o1}}} M_2, \\ M_{2-}^{out} &= M_{2-}^{in} - \sqrt{\frac{1}{\gamma_{o1}}} M_2, \end{aligned} \tag{5}$$

$$\begin{aligned} t = \frac{A_{2+}^{out}}{A_{1+}^{in}} &= e^{i\varphi} + [\gamma_{o1}\gamma_2 e^{e\varphi} + \gamma_o \gamma_1 \\ &+ \sqrt{\gamma_{o1}\gamma_2}(\delta_1 e^{i\varphi} + \delta_2)] . \sqrt{(\gamma_1\gamma_2 - \delta_1\delta_2)} \end{aligned} \tag{6}$$

$$\delta_1 = i\mu_{12} + e^{i\varphi}\sqrt{\gamma_{o1}\gamma_{o2}}, \tag{7}$$

$$\delta_2 = i\mu_{21} + e^{i\varphi}\sqrt{\gamma_{o1}\gamma_{o2}}, \tag{8}$$

where φ is the phase difference between resonators. In conclusion, we can deduce that the transmittance is $T=|t^2|$.

Simulations and Results

To reveal the mechanism of Fano resonance, we utilized the COMSOL multiphysics for the optical structure of GDFDG, transmission spectra and analyzed the results, thus gaining a deeper understanding of Fano resonance.

In this design, UGG and LGG are directly excited by incident light, producing a Fano resonance in the infrared band. Figure 3a, c shows the transmission spectra of the UGG and the LGG. In Fig. 3d, f it is observed that when using the UGG, the electric field is mainly concentrated in the upper layer of

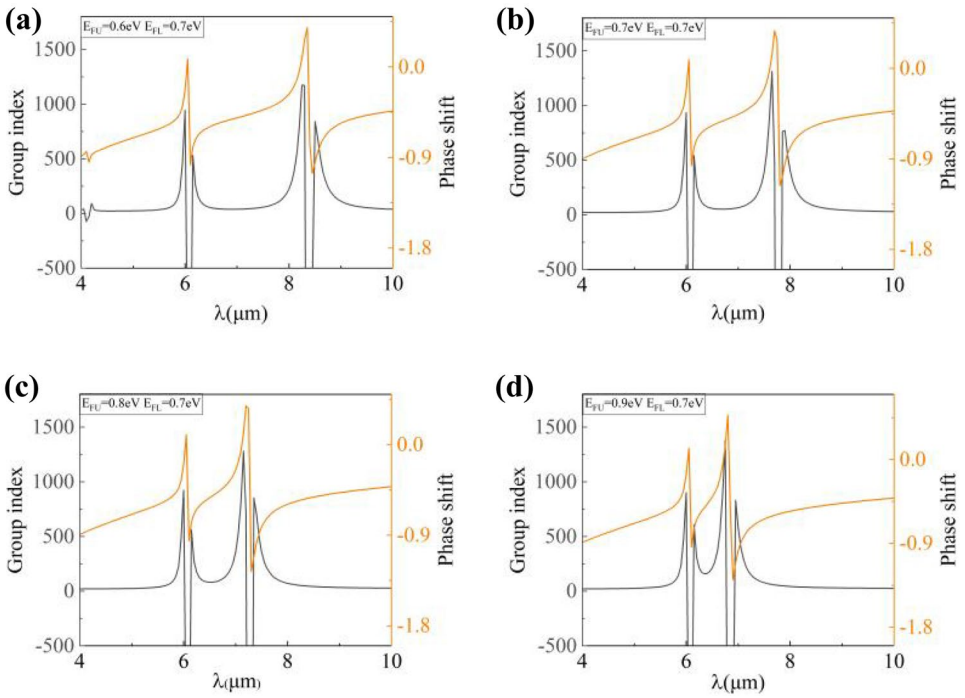

Fig. 6 Schematic diagram of the evolutionary relationship between the phase shift and group refractive index and wavelength, where $E_{FL}=0.7$ eV, $E_{FU}=0.6$ eV, 0.7 eV, 0.8 eV, 0.9 eV, respectively

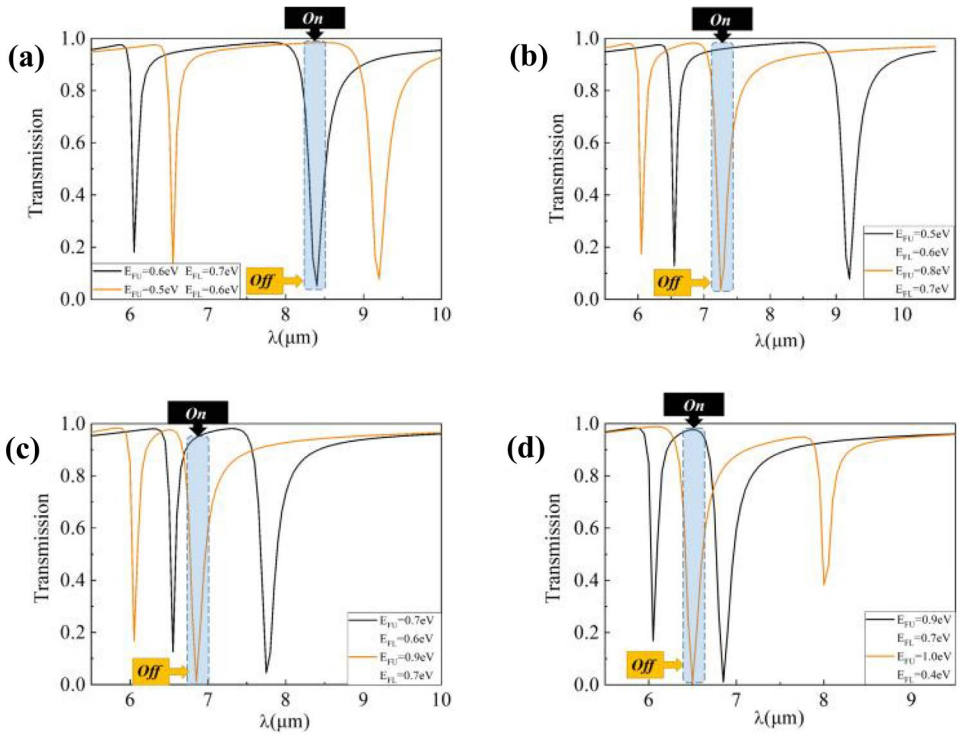

Fig. 7 Schematic diagram of the principle of photoelectric switch

graphene, and in contrast, when it comes to the LGG, the electric field can be found concentrated in the lower layer graphene. Simultaneously, what can be found in Fig. 3b, e is that strong electric fields are distributed on the surface of the upper graphene and the outer edge of the lower graphene, causing a Fano resonance curve, forming a transparent window at a wavelength of 7.55 μm with a resonance of 98.5%. The theoretical fit of the CMT-based transmission spectrum Fano resonance is in good agreement with the simulation results, as shown in Fig. 3b.

Taking the strong dynamic regulation properties of graphene into consideration, PIT can be adjusted by taking full use of it. When fixing the Fermi level of the UGG with the Fermi level of the LGG increasing at a rate of 0.1 eV, as shown in Fig. 4a, peak 1 has a significant redshift and the modulation effect is fantastic. Relatively, when fixing the Fermi level of the LGG and increasing the Fermi level of the UGG at a rate of 0.1 eV, as shown in Fig. 4b, peak 2 has a noticeable redshift, the modulation effect is excellent. Meanwhile, it can also be seen from Fig. 4b that the extinction ratio of the peak2 transmission spectrum can reach 99.2% in the range of 0.5 to 1.0 eV, indicating that the Fano system can be a superior single-band filter. To sum up from the above, we come to a conclusion that the wavelength band and range of the transparent window can be changed by adjusting the Fermi energy level of the upper and lower layers of graphene.

To explore the effect of changing the polarization state on the structure, the relationship between the polarization direction and the transmittance is scanned, as shown in Fig. 5, which illustrates the spectrum is independent of polarization. The reason for this result is that due to the geometric arrangement of the two layers, when the polarization angle θ changes, the excitation efficiency of the upper layer will be compensated by the lower layer so that the polarization of the system is insensitive.

In order to study the application prospects of GDG structure in slow light, numerical simulation was carried out. It is observed in Fig. 6 that the phase shift and the refractive index of the group have a fantastic correspondence, and both have sudden changes at the Fano resonance, which can be illustrated

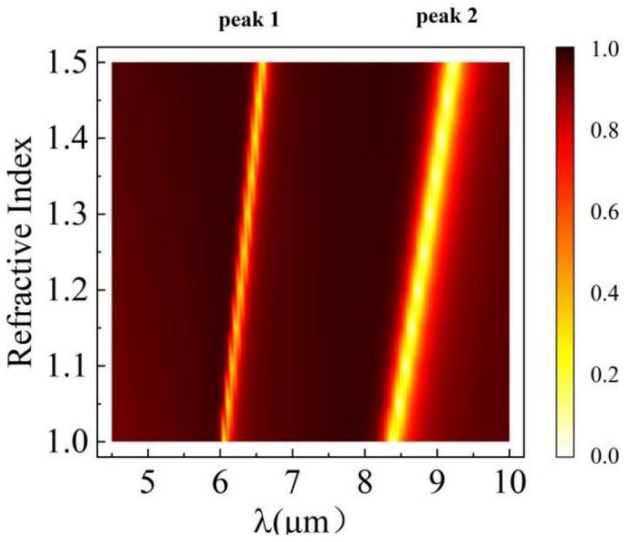

Fig. 8. 3D modulation diagram of refractive index of different environments

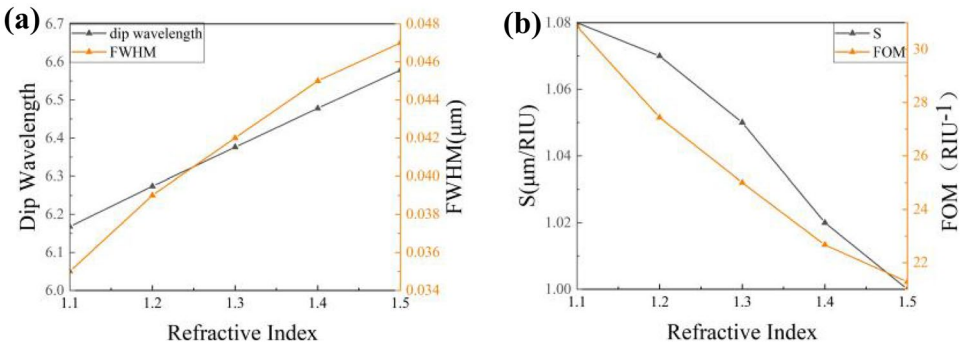

Fig. 9 **a** Dip wavelength and FWHM of GDFDG and **b** *S* and FOM of GDFDG

as high dispersion. Resulted by the destructive interference of the system, not only there will be a high dispersion of the excited plasma waves near the Fano resonance, which manifests itself as a sudden change in the curve, but also induces a distinct phase transition causing the group's refractive index an obvious change. With the increase in the UGG Fermi energy level, the group velocity and phase displacement increase, and the maximum group refractive index reaches 1379 indicating the structure has broad application prospects under slow light conditions.

In addition, based on the characteristics of Fano resonance, whose transmission will be transmitted from the largest to the smallest in very narrow frequency bands, we also studied the optical switching of the Fano system in the infrared band, as shown in Fig. 7. The Fermi energy levels of the UGG and the LGG are changed to obtain optical switches in different wavelength bands.

The transmission spectrum acts as a function of wavelength and Fermi energy, which illustrates the filtering and switching mechanism. Take Fig. 4d as an example, when the UGG Fermi level is 0.9 eV and the LGG Fermi level is 0.7 eV, the emission amplitude T_1 at 6.5 μm is 97.7%, that is, the transmission loss is 2.3%; for the case with the UGG Fermi level is 1.0 eV and the LGG Fermi level is 0.4 eV, the emission amplitude T_2 at 6.5 μm is 0.8%. The high transmittance corresponds to the "on" state in the switch while the low transmittance presents the "off" state, thus it can be set to a switch according to the above situation. The formula for the degree of modulation is $D_M=(T_1\text{-}T_2)/T_1\times100\%$, according to which, the modulation degree D_M in Fig. 7a-d are calculated to be 94.72%, 96.35%, 98.94% and 99.18%, respectively [24].

To investigate whether GDFDG can play a role in sensor components, the relationship between the transmitted spectrum and the refractive index of the environment should be taken into consideration. In Fig. 8, wavelength offset as a function of refractive index values of different media. The resonant wavelengths of peak 1 and peak 2 are linearly related to the refractive index of the dielectric layer, as the refractive index of the environment increases, the transmission spectrum of both formats will get a redshift. We take $S=\Delta\lambda/\Delta n$ to calculate refractive index sensitivity [25].

In order to analyze sensing characteristics, we plot Dip wavelength, full width at half maximum (FWHM), *S* and FOM curves of GDFDG with different refractive indexes [26, 27]. Figure 9a shows that with the increase in refractive index, FWHM of peak 1 gets a slight drop. Therefore, *S max* of the spectra is 1.06 μm/RIU and its FOM reaches 30.86 RIU^{-1} as shown in Fig. 9b. Although the *S max* of peak 2 is 1.7 μm/RIU, the FOM of peak 2 is only 13.39RIU^{-1}. So we do not present the sensing characteristics curves of peak 2 in Fig. 9. Serving as a highly sensitive detection platform, GDFDG may have fantastic application prospects in chemical detection and temperature sensing.

Conclusions

In this paper, a new periodic metamaterial structure GDFDG was established. The CMT and COMSOL multiphysics are employed to analyze its Fano resonance and future application prospects. We use the high dynamic adjustment characteristics of graphene, GDFDG can form a good modulation effect at different wavelengths by adjusting the Fermi energy level of the upper and lower layers of graphene. By analyzing the geometry of the GDFDG and parametric sweep simulations, research shows that the incident of light in different polarization directions does not affect its transmission spectrum. The GDFDG structure has a good application prospect in slow light, for which the maximum group refractive index reaches 1379. Furthermore, what is found is that the main single-band filter and photoelectric switch with a matting rate of near 100% can be obtained via adjusting the Fermi energy level of the upper and lower layers of graphene. Finally, the sensitivity of GDFDG under different environmental refractive indexes manifests that the system was a fairly competitive sensor. In short, this study explores Fano resonance, which lays a certain theoretical foundation for the realization of photoelectric switches, slow light effects and highly sensitive sensors.

Authors' Contributions Z.W. and J.W. contributed to conceptualization and methodology; Z.W. and W.S. contributed to software; J.W. and Z.B. contributed to validation; Z.W, Z.D.H. and J.W. contributed to formal analysis; Z.W., J.W. and Z.H. contributed to writing—original draft preparation; J.S., S.K. and I.S. contributed to writing—review and editing;

Z.W. contributed to visualization; J.W. contributed to supervision; J.W. and S.K. administrated the project; J.W. acquired funding. All authors have read and agreed to the published version of the manuscript.

Funding This work was supported in part by the National Natural Science Foundation of China (11811530052), the Intergovernmental Science and Technology Regular Meeting Exchange Project of Ministry of Science and Technology of China (CB02-20), the Open Fund of State Key Laboratory of Applied Optics (SKLAO2020001A04) and the Undergraduate Research and Innovation Projects of China (2021102Z).

Data Availability The data and material that support the findings of this study are available from the corresponding author upon reasonable request.

Code Availability The code that supports the findings of this study is available from the corresponding author upon reasonable request.

Declarations

Ethical Approval Not available

Consent to Participate The authors declare that they have no conflicts of interest.

Consent for Publication The authors grant the Publisher the sole and exclusive licenses of the full copyright in the Contribution, which license the Publisher hereby accepts. Consequently, the Publisher shall have the exclusive right throughout the world to publish and sell the contribution in all languages, in whole or in part, including, without limitation, any abridgement and substantial part thereof, in book form and in any other form including, without limitation, mechanical, digital, electronic and visual reproduction, electronic storage and retrieval systems, including Internet and Intranet delivery and all other forms of electronic publication now known or hereinafter invented.

Conflicts of Interest The authors declare no conflict of interest.

References

1. Markos P, Kuzmiak V (2016) Coupling between Fano and Bragg bands in the photonic band structures of two-dimensional metallic photonic structures. Phys Rev A 94:033845
2. Bao ZY, Wang JC, Hu ZD, Balmakou A, Zhang C (2019) Coordinated multi-band angle insensitive selection absorber based on graphene metamaterials. Opt Express 27:31435
3. Yao YH, Cheng Z, Dong JJ, Zhang XL (2020) Performance of integrated optical switches based on 2D materials and beyond. Frontiers of Opt 13:129–138
4. Jiang X T, Lu H L, Zhou H, Zhang S D, Zhang H (2018) Epsilon-near-zero medium for optical switcher in a monolithic waveguide chip at 1.9 μm. Nanophoton. 7(11):1835–1843
5. Cheng Y, Chen F, Luo H (2020) Triple-band perfect light absorber based on hybrid metasurface for sensing application. Nanoscale Research Lett 15(1):1–10
6. Feng Y, Li Z, Zhao Q, Chen PP, Wang J (2022) Evaluation of Fano resonance and phase analysis of plasma induced transparency in photonic nanostructure based on equivalent circuit analysis. J of Opt 24:035001
7. Xie H (2021) Dynamic Tunable Plasma-Induced Transparency of Periodic Images of Graphene Nanoribbons. J of Phys 1:012006
8. Lee TM, Loh EW, Kuo TC, Tam KW, Lee HC, Wu D (2021) Effects of ultraviolet and blue-light filtering on sleep: a meta-analysis of controlled trials and studies on cataract patients. Nature 35(6):1629–1636
9. Yoshimi H, Yamaguchi T, Ota Y, Arakawa Y (2020) Slow light waveguides in topological valley photonic crystals. Opt Lett 45(9):2648–2651
10. He Z, Li H, Li B, Chen Z, Xu H, Zheng M (2016) Theoretical analysis of ultrahigh figure of merit sensing in plasmonic waveguides with a multimode stub. Opt Lett 41(22):5206–5209
11. Nong JP, Wei W, Wang W, Lan LL, Shang ZZ, Yi JM, Tang LL (2018) Strong coherent coupling between graphene surface plasmons and anisotropic black phosphorus localized surface plasmons. Opt Express 26(2):1633–1644
12. Qing YM, Ma HF, Cui TJ (2018) Strong coupling between magnetic plasmons and surface plasmons in a black phosphorus- spacer- metallic grating hybrid system. Opt Lett 43(20):4985–4988
13. Zhang XQ, Xu Q, Xia LB, Li YF, Gu JQ (2020) Terahertz surface plasmonic waves: a review. Advanced Photonics 2(1):014001
14. Constant TJ, Hornett SM, Chang DE, Hendry E (2016) All-optical generation of surface plasmons in graphene. Nat Phys 12(2):124–127
15. Zhou W, Zhao D, Shuai YC, Yang H (2014) Progress in 2D photonic crystal Fano resonance photonics. Prog Quantum Electron 38(1):1–74
16. Alonso-Gonzalez P, Nikitin AY, Golmar F, Centeno A (2014) Controlling graphene plasmons with resonant metal antennas and spatial conductivity patterns. Science 344(6190):1369–1373
17. Wang JC, Liu Y, Wang M, Hu ZD, Deng QL (2019) Perfect absorption and strong magnetic polaritons coupling of graphene-based silicon carbide grating cavity structures. J of Phys D 52(1):015101
18. Xu H, Li HJ, He ZH, Chen ZQ, Zheng MF (2016) Influential and theoretical analysis of nano-detect in the stub resonator. Sci Rep 6(1):1–7
19. Li Q, Wang T, Su Y, Yan M, Qiu M (2010) Coupled mode theory analysis of mode-splitting in coupled cavity system. Opt Express 18(8):8367–8382
20. Haus HA, Huang W (1991) Coupled-mode theory. Proc IEEE 79(10):1505–1518
21. Robertson J (2002) Band offsets of high dielectric constant gate oxides on silicon. J of non-crystalline Solids 303(1):94–100
22. Du L, Tang D, Yuan X (2014) Edge-reflection phase directed plasmonic resonances on graphene nano-structures. Opt Express 22(19):22689–22698
23. Rodrigo D, Tittl A, Limaj O, Abajo F, Pruneri V (2017) Double-layer graphene for enhanced tunable infrared plasmonics. Light: Sci Appl 6(6):e16277
24. Liu Z, Gao E, Zhang X, Li H, Xu H, Zhang Z, Luo X (2020) Terahertz electro-optical multi-functional modulator and its coupling mechanisms based on upper-layer double graphene ribbons and lower-layer a graphene strip. New J of Phys 22(5):053039
25. Singh Sekhon J, Verma SS (2011) Refractive index sensitivity analysis of Ag. Au and Cu nanoparticles Plasmonics 6(2):311–317
26. Keshavarz MM, Alighanbari A (2019) Terahertz refractive index sensor based on Tamm plasmon-polaritons with graphene. Appl Opt 58(13):3604–3612
27. Wang JC, Yang L, Hu ZD, He WJ, Zheng GG (2019) Analysis of graphene-based multilayer comb-like Absorption system based-on multiple waveguide theory. IEEE Photon Tech Lett 31:561–564